World Scientific
www.worldscientific.com

An automated multiwell plate reading flim microscope for live cell autofluorescence lifetime assays

Douglas J. Kelly[*,†,§,‖], Sean C. Warren[*,†], Sunil Kumar[*],
João L. Lagarto[*], Benjamin T. Dyer[*,‡], Anca Margineanu[*],
Eric W.-F. Lam[§], Chris Dunsby[*,¶] and Paul M. W. French[*]

[*]Photonics Group, Department of Physics, Imperial College London
South Kensington Campus, London, SW7 2AZ, UK

[†]Institute of Chemical Biology, Department of Chemistry
Imperial College London, South Kensington Campus
London, SW7 2AZ, UK

[‡]National Heart & Lung Institute
Imperial Centre for Experimental & Translational Medicine
Du Cane Road, London, W12 0NN, UK

[§]Department of Surgery and Cancer, Imperial College London
Du Cane Road, London, W12 0NN, UK

[¶]Centre for Histopathology, Imperial College London
Du Cane Road, London, W12 0NN, UK
[‖]douglas.kelly09@imperial.ac.uk

Fluorescence lifetime imaging (FLIM) is increasingly used to read out cellular autofluorescence originating from the coenzyme NADH in the context of investigating cell metabolic state. We present here an automated multiwell plate reading FLIM microscope optimized for UV illumination with the goal of extending high content fluorescence lifetime assays to readouts of metabolism. We demonstrate its application to automated cellular autofluorescence lifetime imaging and discuss the key practical issues associated with its implementation. In particular, we illustrate its capability to read out the NADH-lifetime response of cells to metabolic modulators, thereby illustrating the potential of the instrument for cytotoxicity studies, assays for drug discovery and stratified medicine.

Keywords: High content analysis; FLIM; NADH; metabolism; cisplatin.

1. Introduction

The benefits of automated high content assays are well established for drug discovery and are increasingly recognized for systems biology and basic research in the life sciences. The ability to acquire and analyze fixed point and time-lapse image data across cell populations with minimal supervision and medium to high throughput creates opportunities to screen complex biological phenotypes against compound and gene libraries, to test drug candidates and to explore disease mechanisms. In particular, the capacity to increase the number of cells that can practically be imaged and the number of "repeats" per condition in a single "experiment" mitigates for biological noise, with the ability to average readouts over large datasets enabling quantitative measurements of challenging assays such as protein–protein interactions to become statistically robust. To this end, high content analysis (HCA) has evolved from simple automated intensity-based imaging to utilize spectroscopic image-based readouts of sample arrays, particularly harnessing the molecular specificity of fluorescence labeling. This paper concerns the emerging application of fluorescence lifetime imaging (FLIM) to HCA, which has previously been used to provide high content readouts of Förster resonance energy transfer (FRET) and offers the potential to screen interactions of proteins labeled with exogenous, genetically encoded donor fluorescent fusion proteins.[1–3] FLIM can also be used to gain insight into cellular processes via the autofluorescence lifetimes of endogenous cellular fluorophores and we report here the translation of such readouts to an automated FLIM plate reader.

One key endogenous cellular fluorophore is reduced nicotinamide adenine dinucleotide (NADH). NADH is an important coenzyme in cellular metabolism, being a product of glycolysis and the citric acid cycle and a substrate for the generation of ATP by oxidative phosphorylation. NADH is fluorescent under UV excitation and this property has been studied for more than 50 years with the goal of linking changes in metabolic state to concomitant changes in fluorescence parameters measured *in vivo*.[4] In addition, *in vitro* studies of the fluorescence enhancement of NADH upon interaction with binding partners have been used to quantify the activity of dehydrogenase enzymes.[5] This readout results from the binding of NADH in an elongated conformation that reduces quenching of the reduced

nicotinamide group by the adenine moiety.[6] In 1992, Lakowicz *et al.* imaged the fluorescence lifetime of NADH upon protein binding,[7] indicating the potential for FLIM of NADH to be used in biological contexts. Crucially, measurements of excited-state lifetimes do not depend on total fluorophore concentration, detection efficiency or sample absorption; therefore time-resolved fluorescence data from different instruments can be directly compared and may be applied to live cell imaging experiments and translated to both *in vivo* pre-clinical and clinical measurements. Over the past two decades the literature relating to fluorescence lifetime measurements of NADH, both *in vitro* and *in vivo*, has grown extensively, with many studies across different cell lines and utilizing different metabolic modulators establishing a link between changes in fluorescence lifetime and changes in cell metabolism.[8–11] Since aberrant metabolism is a hallmark of cancer, there has been considerable interest in exploiting measurements of cellular autofluorescence lifetime to read out changes in metabolic state for the study, diagnosis and monitoring of cancer; such changes have been associated with a shift from oxidative phosphorylation to glycolysis.[12] Recently, the link between metabolic state and stem cell fate has offered an additional motivation for exploiting NADH lifetime-based readouts.[13–17]

FLIM is most commonly implemented in laser scanning confocal or multiphoton microscopes using time-correlated single photon counting (TCSPC). This can be directly applied to HCA,[2] but the need for FLIM to detect significantly more photons/pixel than are required for intensity-based imaging makes this approach, where image data are acquired sequentially (with the maximum imaging rate limited by considerations of photobleaching, phototoxicity and sometimes by fluorescence protein expression level), too slow for many HCA applications. FLIM-based FRET readouts have been utilized in HCA using wide-field frequency modulated imaging[1,18] or time-gated detection with Nipkow disk-based optical sectioning.[3,19] to realize automated acquisition of fluorescence lifetime images across an array (multi-well plate) requiring only ~10 s/field of view. Automated FLIM assays have included interrogation of post-translational modifications downstream of epidermal growth factor receptor (EGFR),[1] a small-scale screen of inhibitors for internalization of the transmembrane receptor CXCR4[2] and an investigation of the effects of N-myristoyltransferase inhibitors on

Gag protein aggregation in HIV models.[3] To date, however, such rapid automated FLIM technology has not been applied to assays utilizing endogenous fluorophores. To the best of our knowledge, we present here the first demonstration of automated widefield time-gated FLIM being applied to readouts of changes in cellular metabolism as reported by the fluorescence of reduced NADH. We outline practical challenges associated with UV-excited FLIM, including background fluorescence and cell viability, which were addressed in the design of this instrument. We then present its application to quantitative measurements of NADH lifetime parameters to read out protein binding and changes in cellular metabolism induced by a metabolic inhibitor (rotenone) and an anti-tumor drug (cisplatin).

2. Materials and Methods

2.1. *Imaging instrumentation and data acquisition software*

Pulsed UV excitation light at 370 nm was obtained from a frequency doubled femtosecond mode-locked Ti:Sapphire laser (MaiTai HP with #3980 Frequency Doubler/Pulse Selection Unit, SpectraPhysics). Excitation intensity was controlled by means of a motorized filter wheel (FW102B, Thorlabs) fitted with neutral density filters. Excitation radiation was coupled to the back port of an inverted epifluorescence microscope frame (IX-81, Olympus) via a UV-transmitting multimode fiber (M67L02, Thorlabs) followed by a lens system and a spinning disk diffuser of UVT acrylic (Luminit) to provide spatially incoherent wide-field illumination, as shown in Fig. 1. This configuration ensures maximum flexibility for coupling different laser sources into the plate reading microscope. The microscope frame was equipped as described previously[3] with optical autofocus, motorized stage, automated objective nosepiece and camera port selection. A $40\times$, 0.6 NA objective lens (LUCPLFLN $40\times$, Olympus) was used that was specified for UV excitation and offered a long working distance that was compatible with a range of different multiwell plates. On the left hand port, a gated optical intensifier (GOI) (HRI, Kentech, with an S20 photocathode for high sensitivity in the blue spectral region) provided time-resolved imaging capabilities, with the phosphor output being read out using a cooled CCD camera (ORCA ER-II, Hamamatsu). The spatial resolution of this FLIM
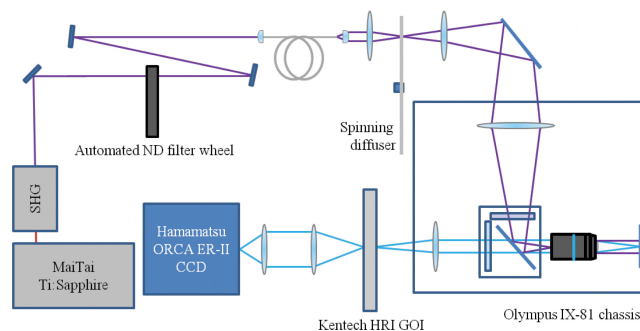

Fig. 1. Schematic of experimental configuration of plate reader equipped for autofluorescence lifetime imaging. The microscope chassis is equipped with motorized stage, filter cube cassette and objective nosepiece as well as an autofocus unit to facilitate automated acquisition. Time resolved imaging is implemented using a GOI. (SHG: second harmonic generation, ND filter: neutral density filter, GOI: gated optical intensifier).

set-up was limited by the GOI rather than the optical components or camera pixel size. The GOI can resolve 18 line pairs/mm and so features as small as $1.4\,\mu$m may be resolved in the sample plane. A nonFLIM imaging capability was implemented by attaching a second CCD camera (Flea2 08S2M, Point Grey Research) to the microscope trinocular with a lens relay designed to compensate for the difference in chip size and so match FLIM and non-FLIM fields of view. A white light LED provided illumination for bright field or phase contrast imaging and was controlled using a digital acquisition card (USB6008, National Instruments) and an LED driver (LEDD1B, Thorlabs). A syringe pump (KD Scientific) could be attached to the system for automated stimulation of samples during time course experiments. The microscope is fitted with an incubator (Solent Scientific) to facilitate live cell imaging at 37°C.

The instrument's acquisition software was written predominantly in LabVIEW (National Instruments) and was designed to allow the user to control all aspects of FLIM data acquisition on the plate reader including camera parameters, gate delays and filter sets. The software allows the user to design automated experiments including movement to different fields of view, time-lapse imaging, imaging in multiple z-planes and phase contrast imaging, all of which can be combined in arbitrary sequences. To minimize the light dose, exposure to the excitation laser was controlled by automatically shuttering the laser during the autofocus routine, during stage translation and when the acquisition is paused between time-lapse images. The acquisition software

permits automatic upload to OMERO[20] servers for image data storage, sharing and subsequent analysis.

To minimize the overall data acquisition time and light exposure, a cell "pre-find" function was implemented in the experimental protocol to automatically identify the most suitable fields of view for subsequent FLIM, as has been described previously for our FLIM plate reader.[19] For this work, the software was modified to enable cell searching to be performed at lower (e.g., $10\times$) magnification than the FLIM readouts, thereby increasing the speed of identification of suitable fields of view. For autofluorescence-based studies, the pre-find function has been adapted to work with phase contrast images, in which regions of cells are identified using a variance thresholding technique[21] implemented in LabVIEW. Since this method fails most often when searching near the edge of wells, where the vertical sides of the wells and the meniscus of the imaging media degrade phase contrast image quality, the search routine is typically started from the center of each well in turn. This is successful for all but the sparsest samples. If necessary, more complex cell identification functionality could be employed using CellProfiler,[22] an open source cell image analysis software package, which can be called from the pre-find tool, although this capability was not used for the work presented here.

2.2. *Imaging parameters*

Data presented here were collected under excitation at 370 nm, with excitation power after the objective measured to be in the range 95–115 μW. Excitation light was directed to the sample via a filter cube (Semrock 377/50 excitation, 409 dichroic, 409LP emission) with an additional barrier filter (Semrock, 440/60) being used to select for NADH fluorescence over background. The total acquisition per field of view is typically < 25 s, depending on the acquisition parameters: hardware autofocusing generally requires ~ 3 s while 2–3 s are required to switch between FLIM and phase contrast imaging when performed as part of the automated acquisition. Fluorescence decays are sampled at eight time delays after pulsed excitation and the CCD integration times and frame accumulations are optimized for each specific sample to maximize dynamic range and avoid saturation. For data presented here, the typical total exposure per field of view to excitation laser light is 10–20 s.

For preliminary experiments to investigate cell viability, cells stained with Erythrosin were imaged at $10\times$ magnification using a standard fluorescence microscopy configuration (mercury lamp, 545/30 excitation; 610/75 emission) as well as bright field illumination.

2.3. *Sample preparation*

2.3.1. *Cell culture and imaging conditions*

MCF7 cells (ECACC, cat. no. 86012803) were grown under standard conditions (37°C, 5% CO_2). Growth media comprised DMEM containing phenol red and glucose (4.5 g/L) supplemented with 2 mM glutamine, 10% fetal bovine serum (FBS) and 1% penicillin-streptomycin. Imaging was carried out in Hank's Balanced Salt Solution (HBSS) supplemented with 2 mM glutamine, 4.5 g/L glucose and 10 mM HEPES (4-(2-hydroxyethyl)-1-piperazineethanesulfonic acid) buffer. Live cell imaging was conducted at 37°C.

2.3.2. *Protein binding assay to demonstrate repeatability*

Stock solutions of βNADH (Sigma-Aldrich) and mitochondrial malate dehydrogenase (mMDH, Merck-Millipore) were prepared in Dulbecco's phosphate buffered saline (DPBS) without calcium or magnesium (Invitrogen) at room temperature. Concentrations were calculated based on absorption measurements performed using a spectrophotometer (UV3101-PC, Shimadzu). Final solutions for lifetime measurements were made up further in Mg/Ca negative DPBS, with βNADH concentration held constant at 50 μM, whilst the concentration of mMDH was varied between 0 and 12.1 μM. 50 μL of solution was pipetted into wells of a glass bottomed 96-well plate (Imaging Plate CG, zell-kontakt GmbH) in a step pattern.

2.3.3. *Vital dye exclusion assay*

MCF7 cells were split into 1:3 one day prior to seeding on a glass bottomed 96-well plate in standard growth media at a density of 10^4 cells per well. 24 h post seeding, growth media was aspirated and replaced with imaging media following washing with DPBS. Erythrosin viability staining was performed following the protocol for adherent cells outlined in Krause *et al.*[23] Briefly, erythrosin B was

prepared at $5\,\mu g/mL$ in growth media, in which cells were then incubated at room temperature for 2 min before washing three times with imaging media. To confirm the effectiveness of the staining method, the cells were subjected to "partial heat-shock" as a positive control, following Krause *et al.*[23]: Cells were submersed in 60°C DPBS for 10 s, then 0°C DPBS for 5 s before staining. DPBS was heated to 60°C using a water bath. Low temperature DPBS was thawed from frozen immediately prior to the experiment. Temperatures were checked (to within 2°C) using a thermocouple. DPBS was introduced to wells by pipetting down the side of wells to minimise mechanical disruption of cell adhesion. All measurements were made at 37°C, in imaging media.

2.3.4. *Assay of action of rotenone on live MCF7 cells*

MCF7 cells were seeded under conditions outlined in Sec. 2.3.3; here, $100\,\mu L$ imaging media was added to wells to replace growth media 24 h post seeding. Rotenone (R8875, SigmaAldrich) was prepared from powder in ethanol to 1 mM, and further diluted in imaging media to $2\,\mu M$. Ethanol was added in a ratio 1:500 to imaging media to make control stimulation media. Both rotenone and control media were maintained at 37°C prior to stimulation being delivered by the automated liquid handling system during a time course acquisition. Imaging was performed at 37°C.

2.3.5. *Assay of action of cisplatin on live MCF7 cells*

MCF7 cells were seeded under conditions outlined in Sec. 2.3.3. Cells were incubated for 24 h post seeding before any treatment was started. Growth media was replaced 24 and 6 h prior to imaging with cisplatin-supplemented growth media at varying concentrations. 24 h after treatment was started, growth media was aspirated and replaced with imaging media following washing with DPBS. All measurements were made at 37°C.

2.4. *Data analysis*
2.4.1. *FLIM data*

To fit our experimental data to a double exponential decay model, we make use of the global fitting capabilities of *FLIMfit*, an open source analysis package described elsewhere.[24] Briefly, lifetime data can be efficiently and robustly fitted to multi-exponential models by global analysis based on variable projection. Complex decay models can thus be globally fitted across an image, a time series or a number of repeat acquisitions for a specific condition (e.g., "dose"). Furthermore, *FLIMfit* enables models to be adjusted to account for instrument response functions, incomplete decays resulting from repetitive pulsed excitation and spatially varying and time varying backgrounds. For the datasets presented here, such simultaneous global fitting of millions of pixels in parallel typically requires less than a minute of computation time using *FLIMfit* running on a standard desktop computer.

Before fitting, an intensity threshold criterion was applied to FLIM images in order to analyze only the pixels corresponding to cells. The lifetime data was smoothed with a 3×3 square kernel before fitting, and reference reconvolution methods were used to account for the instrument response function[25] using Stilbene 3 (a monoexponential dye, $\tau = 1200\,ps$) as a lifetime reference. This approach to fitting time gated FLIM data has been validated by simulation. Time-varying fluorescent background originating from the multiwell plate or from media components (Sec. 3.1) was accounted for using a fluorescence decay profile measured from a well without seeded cells. For consistency with previously published literature, mean lifetimes are presented as "amplitude-weighted" means ($\tau_m = \beta_1\tau_1 + \beta_2\tau_2$). When applying global fitting across the experimental data presented here, errors are typically shown as standard errors calculated across repeat wells within a condition. Where relevant, significance of difference in measured parameters is tested using Tukey's honestly significant difference criterion for multiple comparisons following one-way analysis of variance (MATLAB, MathWorks).

2.4.2. *Vital dye exclusion data*

Analysis was performed in ImageJ: fluorescence images were thresholded and overlaid on phase contrast images in order to determine the fraction of cells that had been stained. Counting of cells was performed manually. Results from imaged and heat shocked cells were compared to control results using Dunnet's test, implemented in MATLAB.[26]

3. Results

3.1. *Background fluorescence characterization*

In contrast to multiphoton microscopy of NADH, which is inherently optically sectioned, wide-field single photon excitation measurements of NADH autofluorescence lifetime are prone to background fluorescence, which might arise from UV excitation of fluorescence in the microscope optics, sample holders (e.g., multiwell plates, cover slips, etc.) and culture media. In Fig. 2(a), we present an overview of the measured intensity of selected sample holders described in Table 1 under the experimental conditions outlined in Sec. 2.2. Well plates with plastic bases rather than glass are preferred in visible-wavelength studies, as cells grown on plastic tend to exhibit improved adhesion and morphology and in our hands show superior expression of transfected protein constructs. However, under UV illumination, plastic surfaces present unacceptably high background fluorescence, contributing 40% of the number of counts of a typical cell sample. In contrast, background from glass substrates contributes less than 5% of cell fluorescence. Figure 2(b) illustrates the fluorescence intensity originating from different components of media, for which growth media and imaging media formulations are outlined

Table 1. Sample holder parameters.

Product name	Supplier	Base material	Base thickness (μm)
Cover glass	VWR	Borosilicate glass	160
Imaging plate CG	ZellKontakt	Borosilicate glass	145
Matriplate microplate	GE Healthcare	Borosilicate glass	720
μClear 96 well	Greiner BioOne	μ Clear® film	190
Nunc 384 optical bottom	Thermo Fisher	Polystyrene/ polymer	250

in Sec. 2.3.3, and all drug treatments are diluted in imaging media. Based on these results, we choose to use glass-based well plates in all UV-wavelength plate reader experiments, and avoid imaging in media with either phenol red or FBS.

3.2. *Protein binding assay to demonstrate repeatability*

Experiments using mixtures of free and mMDH bound NADH in aqueous solution were used to verify the repeatability of lifetime measurements performed under UV excitation across a 96-well
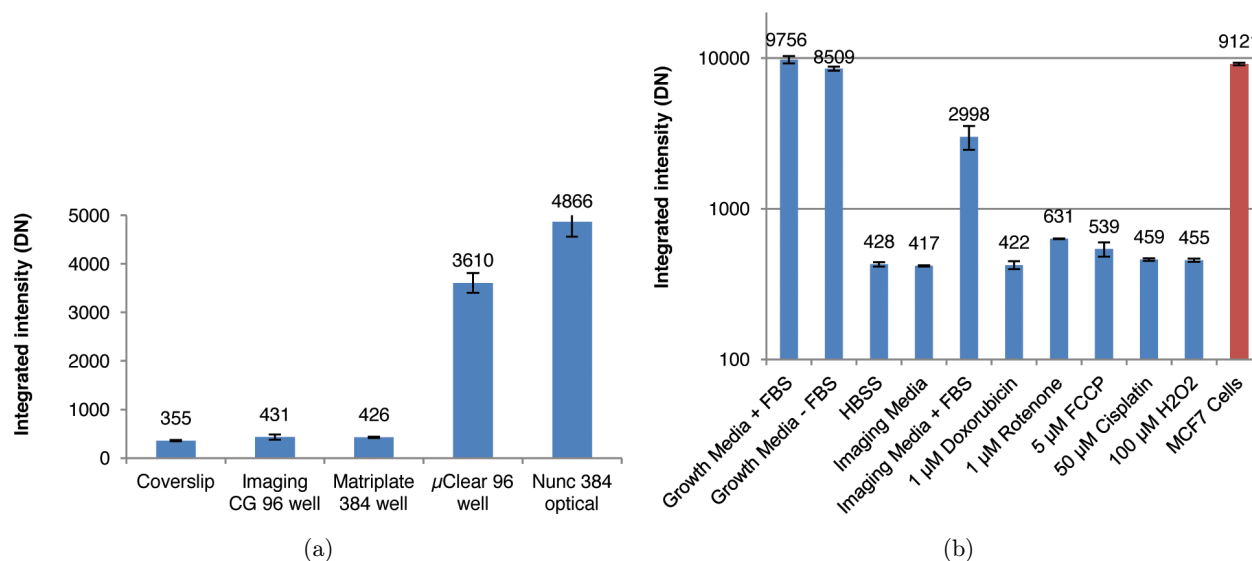

(a)

(b)

Fig. 2. Comparison of relative contributions from different potential sources of background fluorescence. (a) Integrated fluorescence intensity in units of camera digital numbers (DN) originating from a range of sample holders. (b) Comparison of background signal from media components and treatment compounds. Blue bars show integrated intensity originating from media components, including signal from Matriplate 384 well; red bar shows integrated intensity from MCF7 cells for comparison. Error bars show standard deviation across repeat wells.
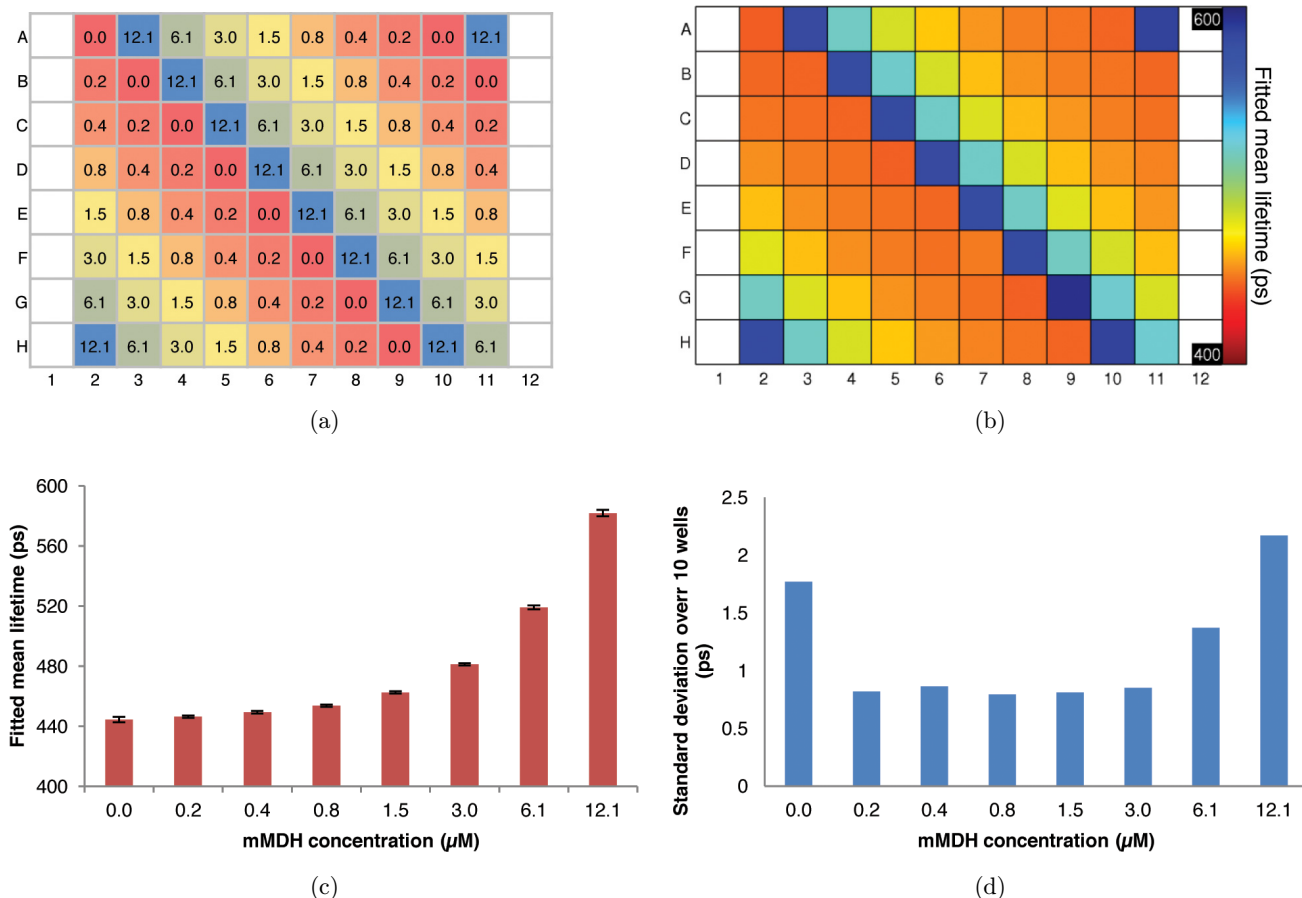
Fig. 3. Results showing repeatability of lifetime results across a 96-well plate. (a) Map showing plating layout for NADH–mMDH measurements of lifetime repeatability; numbers associated with wells represent mMDH concentrations in μM. (b) Plate map of mean fitted lifetime across each well. (c) Plots showing fitted mean lifetime averaged over repeat wells. (d) Standard deviations across repeat wells to illustrate how repeatable are the lifetime measurements between repeat wells.

plate populated as shown in Fig. 3(a). The results shown in Figs. 3(b) and 3(c), for which the standard deviations in fitted mean lifetime across multiple wells are shown in Fig. 3(d) to be less than 2.5 ps, indicate that the measurements of NADH lifetimes are highly reproducible across repeat wells. Comparing Figs. 3(a) and 3(b), it can be seen that the measured lifetime varies according to the expected pattern of solutions across the plate. The uniformity of the measured fluorescence lifetime across different spatial positions within the plate, as seen in Fig. 3(b), indicates that there are no spatial variations in background fluorescence, e.g., due to edge effects, and no time-dependent change in background fluorescence, for example originating in the microscope objective, that would otherwise skew results based on time of acquisition, which is linked to position within the plate.

3.3. *Vital dye exclusion assay*

An investigation was conducted to establish that the UV excited fluorescence imaging process did not lead to cell death due to phototoxicity. Cells were prepared as outlined in Sec. 3.3 above and imaged over a 135-min period to approximate the duration of a typical multiwell plate experiment. Typical imaging parameters (0.1 mW excitation power at sample for 10 s) were used with each field of view being imaged twice. After imaging, cell death was quantified in four wells that had been imaged with UV excitation, four wells that had not been imaged and four wells that had not been imaged but had been "partially heat-shocked". The cell treatment, staining and image analysis is described in Secs. 2.3.3 and 2.4.2. Cells that had been imaged with UV excitation showed no significant increase in staining fraction over those that had not been imaged. Cells in the wells exposed to the positive

(a)
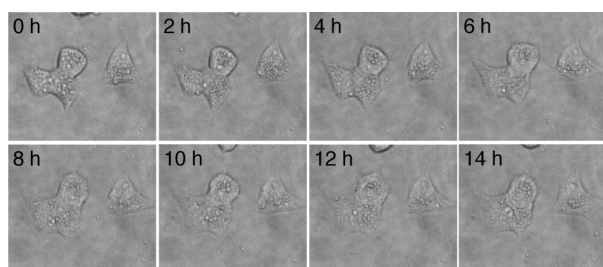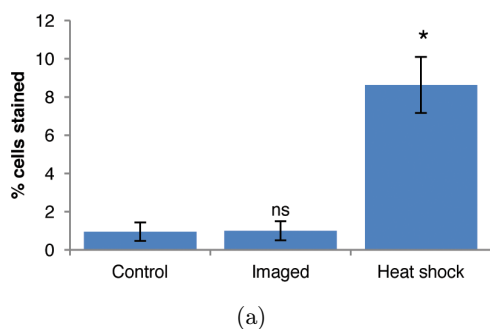
(b)

Fig. 4. Results of vital dye exclusion and morphology assays following autofluorescence imaging experiments. (a) Results of erythrosin viability staining for adherent cells, illustrating that no significant difference is evident between control and imaged cell viability using this method. (b) Exemplar phase contrast images over a 16-h time course that were interleaved with NADH autofluorescence FLIM acquisitions; the time elapsed since start of experiment is indicated in hours. There are no changes in cell morphology to indicate adverse effects caused by this extended imaging.

control "partial heat shock" condition exhibited a significant increase in staining fraction over both imaged and nonimaged conditions [see Fig. 4(a)].

In a separate experiment, BT474 cells were imaged every 2 h over a 16-h time course with phase contrast imaging and autofluorescence imaging being interleaved in order to simulate a time-lapse experiment and look for changes in cell morphology that might indicate cell damage. Figure 4(b) shows time lapse phase contrast images acquired across this period for which no adverse effects are apparent from changes in cell morphology.

3.4. Assaying metabolic modulation: Action of rotenone on live MCF7 cells

Rotenone is a known inhibitor of Complex I in the respiratory chain. As such, rotenone treatment is expected to result in an increase in free intracellular

NADH, and hence a decrease in mean autofluorescence lifetime. 100 μL of either control media or rotenone sufficient to reach a final concentration of 1 μM was automatically dispensed immediately prior to imaging the fourth time point in a time course for each well in turn. Autofluorescence lifetime data were collected across six wells per condition, for each of which automated time courses were taken in sequence. Figure 5 presents the time series of the autofluorescence lifetime images and mean NADH lifetime values averaged over the
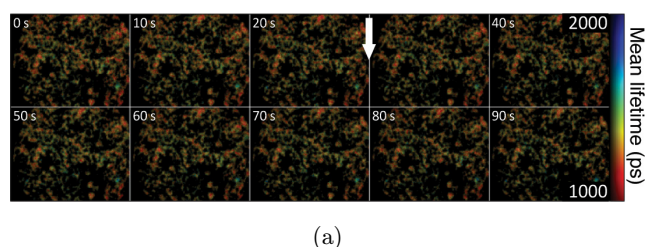
(a)
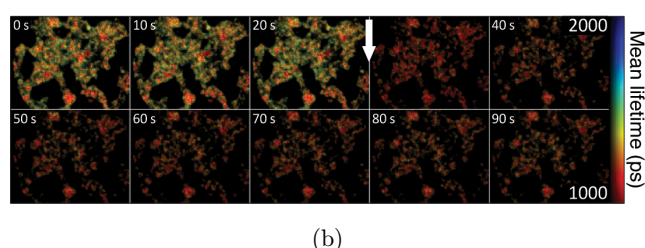
(b)
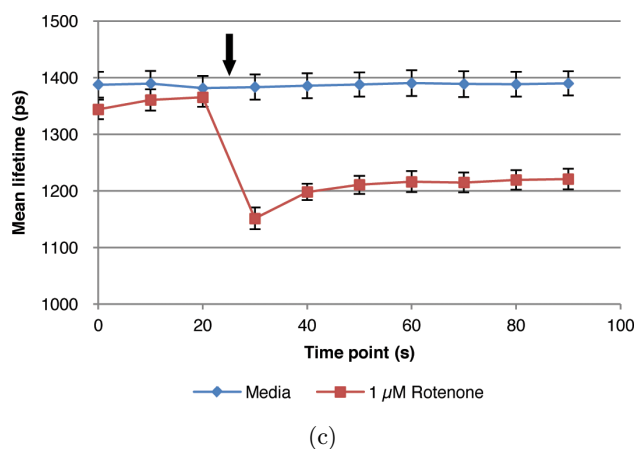
(c)

Fig. 5. Results showing effect of 1 μM rotenone on MCF7 cells. (a) Intensity merged mean lifetime images across time points from a single well, with control media added after third time point as illustrated. (b) Intensity merged mean lifetime images across time points from a single well with rotenone being added after third time point (scale bar = 100 μm). (c) Mean fitted lifetimes across six wells of each condition plotted against time point. Arrow indicates addition of control media or rotenone; error bars show standard errors calculated across repeat wells.
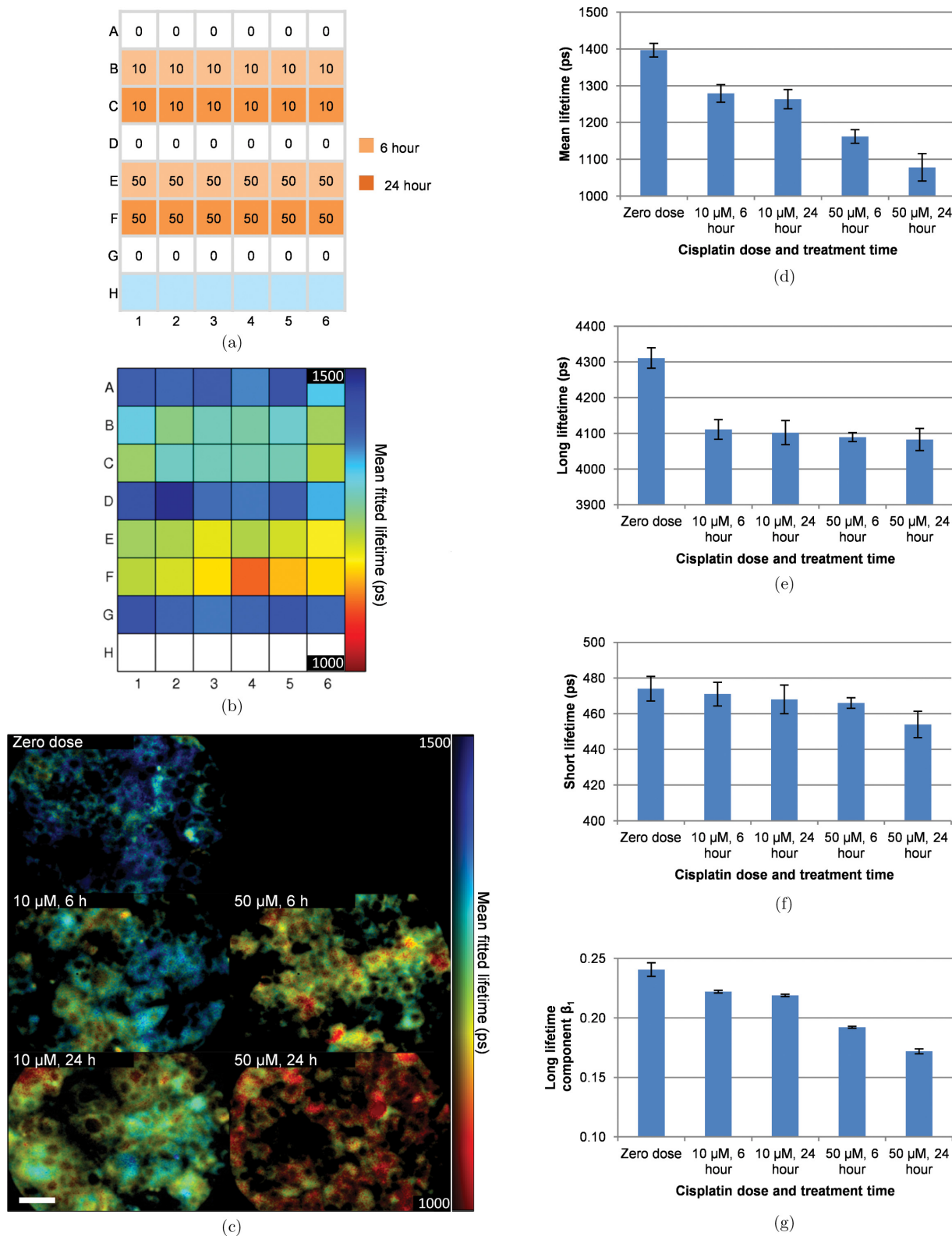
Fig. 6. Results showing effect of cisplatin treatment dose and time on MCF7 cells. (a) Plate map indicating cisplatin treatment dose and time. (b) False-color map showing mean fitted lifetimes obtained for each well across the plate. (c) Exemplar intensity merged FLIM images from the dataset with false color scale showing fitted mean lifetime (scale bar $= 50\,\mu$m). (d)–(g) Fitted parameters presented by condition with error bars representing standard errors over repeat wells.

repeat wells with the standard errors being calculated across the repeat wells. No change in lifetime is observed when control media is added to the wells, showing that the act of dispensing liquid into wells alone has no effect on the lifetime measurement. In contrast, there is a significant decrease in measured lifetime upon stimulation with $1\,\mu$M rotenone. The observed reduction in mean lifetime is consistent with previous studies in which oxidative phosphorylation has been inhibited by Complex I poisoning[8] and may reflect an increase in free NADH in the cell.

3.5. *Assaying metabolic modulation: Action of cisplatin on live MCF7 cells*

A plate for investigating NADH lifetime readouts of time- and dose-dependent responses to cisplatin treatment was designed as shown in Fig. 6(a). MCF7 cells were imaged at 37°C in imaging media described in Sec. 2.3. Cells were sufficiently densely seeded such that no pre-find operation was required and the first 10 fields of view spiraling outward from the center of each well were imaged. Figures 6(d)–6(g) present data for cells untreated or treated with cisplatin 6 or 12 h before being imaged with mean lifetime values obtained from global fitting to a double exponential decay model across the images in each well. Figures 6(b) and 6(d) show the changes in mean autofluorescence lifetime obtained from global fitting to a double exponential decay model across all the images for each condition (i.e., across repeat wells) and indicates a significant decrease in mean autofluorescence lifetime following cisplatin treatment. Figures 6(e) and 6(f) show the variation of the short ("free NADH") and long ("bound NADH") lifetimes with cisplatin dose and exposure time and Fig. 6(g) shows the corresponding changes in the fractional contribution from the long ("bound NADH") component to the autofluorescence signal, which decreases with increased cisplatin dose and treatment time. According to Tukey's test, the short lifetime components measured in this experiment and the long lifetime components of the cisplatin treated cells do not vary significantly for different cisplatin treatments, although all the cisplatin treated cells present a significantly shorter long component ("bound NADH") lifetime than the untreated cells.

4. Discussion

The work reported here aimed to investigate the potential to apply an automated wide-field FLIM plate reader to readouts of cellular autofluorescence with a view to developing high-content FLIM assays for toxicology and to explore potential pitfalls of this approach. Currently, cellular autofluorescence FLIM experiments are typically performed using laser scanning multiphoton microscopes with lifetimes determined using TCSPC. Such measurements benefit from being optically sectioned, which enables intracellular autofluorescence to be spatially separated from other components that can present an unwanted background. However, the need to sequentially scan the excitation spot limits their applicability to high throughput studies since the nonlinear scaling of multiphoton photobleaching and photodamage with excitation intensity precludes the use of the high excitation powers required for rapid imaging. The parallel pixel acquisition of wide-field time-gated FLIM does enable high imaging speed/ throughput but, as indicated by the results presented in Sec. 3.1, the composition of media in which cells are imaged and the choice of growth substrate are important considerations for wide-field FLIM due to their potential contributions to background fluorescence when there is no optical sectioning. Here we show that appropriate selection of media components and substrates can permit quantitative wide-field FLIM experiments with minimal "background" contribution to fluorescence decays. The imaging media composition outlined in Sec. 2.3.1 allows FLIM experiments to be performed over extended time periods while maintaining a stable metabolic state in control samples (data not shown).

Using glass bottomed well plates and media optimized for minimal UV-excited fluorescence, the results in Sec. 3.2 assaying binding of NADH to mMDH in solution show that our FLIM plate reader achieves a high level of repeatability across a 96-well plate, validating the use of such an instrument for quantitative lifetime-based studies of UV excited fluorescence. The vital dye exclusion assay presented in Sec. 3.3 shows that the number of dead cells does not increase following imaging with pulsed UV excitation in our wide-field instrument and the extended time course FLIM measurements do not result in changes in cell morphology indicative of cell deterioration, as determined by the phase contrast imaging interleaved with the FLIM acquisition.

While further experiments would be required to determine the precise photochemical impact of the UV illumination on live cells, e.g., the potential generation of reactive oxygen species or DNA damage, the results presented here give us confidence that the UV excitation is not significantly compromising the health of the cells being imaged.

To realize quantitative FLIM-based assays of changes in metabolism using cellular autofluorescence, it is necessary to deal with complex fluorescence decay profiles, including contributions from free and bound metabolites. Throughout this work we have analyzed NADH fluorescence by global fitting to a biexponential decay model and have accounted for background fluorescence, instrument response and incomplete decays in the fitting procedure, as outlined in Sec. 2.4.1. However, we note that NADH exhibits a more complex fluorescence decay profile for which the fitting of FLIM data is subject to some discussion in literature. It is generally accepted that free NADH in solution has two lifetime components associated with different conformations of the molecule: folded (quenched) and extended (unquenched).[27] The lifetimes of these components of NADH can be affected when binding to proteins and can vary depending on binding partner.[28,29] There is potentially an additional source of cellular autofluorescence detected in our experiments arising from NADPH, which is spectrally indistinguishable from NADH, although it is normally considered that the relative abundance and quantum yield of NADPH is sufficiently low that it may be ignored.[30] Thus, a complete description of NADH fluorescence would require a multiexponential model with four or more components. With the limited number of autofluorescence photons typically detected, however, it is generally not possible to fit FLIM data to such complex models. Qualitative differences between different NADH signals can be obtained by fitting to a single exponential model but double exponential models result in better fits to experimental data (i.e., lower χ^2) and so the mean lifetime calculated from a double exponential fit is often used as a more reliable readout of changes in metabolism. To relate lifetime measurements to underlying metabolic changes, the short and long lifetime components of a double exponential fit are often considered to represent the free and bound NADH components, respectively.[7,31] Alternatively, it is possible to avoid the challenges associated with nonlinear iterative fitting photon-limited data to complex models by using phasor analysis,[32] although for quantitative readouts the resulting phasor plots need to be interpreted as linear combinations of lifetime components of a chosen model, typically representing bound and free NADH.

Figure 5 illustrates the application of a double exponential fit to NADH autofluorescence decay profiles where the variation in the mean lifetime provides a readout of the action of rotenone on live MCF7 cells. Rotenone acts to inhibit oxidative phosphorylation by poisoning Complex I in the electron transport chain and previous studies have shown that rotenone causes a reduction in the mean lifetime.[8] A similar reduction has been shown in studies using cyanide compounds[33,34] that act by inhibiting Complex IV. The observed decrease in measured autofluorescence lifetime upon rotenone stimulation evident in Fig. 5 indicates that our automated FLIM plate reader can report changes in NADH autofluorescence lifetime caused by inhibition of oxidative phosphorylation.

To illustrate the potential of automated FLIM assays for studies of toxicology and drug efficacy, we investigated the action of cisplatin on live MCF7 cells. Cisplatin is a drug commonly used in anti-cancer therapies, being potent against a great number of tumors. The mode of action of cisplatin is primarily through the formation of DNA adducts and double strand breaks that result in the activation of signaling pathways that ultimately lead to apoptosis.[35–37] In previous work, glycolysis in MCF7 cells has been shown to increase following treatment with cisplatin[38] and we therefore investigated whether treatment with cisplatin could lead to a change in the NADH fluorescence lifetime parameters. Our preliminary results presented here in Sec. 3.5 are consistent with changes in NADH fluorescence lifetime parameters following a shift in cell metabolism toward glycolysis reported by Skala *et al.*[39] We note, however, that apoptosis induced by staurosporine has previously been linked to an increase in mean NADH fluorescence lifetime.[30,40] The difference between this observation and our results may be due to the specific modes of action of cisplatin and staurosporine and/or the rate at which apoptosis occurs with these two compounds but further work would be required to elucidate this.

5. Conclusions

We have reported the development and demonstration of what we believe to be the first automated

multiwell plate reading FLIM microscope for application to autofluorescence lifetime imaging under wide-field UV illumination. We have shown that wide-field time gated imaging can be applied to quantitative automated FLIM-based readouts of NADH fluorescence, noting that wide-field FLIM provides greater signal-to-noise per unit acquisition time than laser scanning TCPSC systems,[19] making it more practical for "high throughput" unsupervised lifetime imaging-based multiwell plate assays. To illustrate its potential for assays of cellular metabolism, we have validated its reproducibility using solution-based experiments and presented exemplar measurements of the action of metabolic modulators in live cells.

We believe the automated FLIM plate reader reported here is already useful for reading out changes in cell metabolism without the need for exogenous staining. Lifetime-based readouts of cellular autofluorescence can provide information on metabolite binding states that is not available from intensity measurements and the ratiometric character of FLIM enables such readouts to be translated across imaging platforms[41] and directly correlated with *in vivo* measurements. We envisage that its implementation on a high content imaging platform can extend FLIM of cellular autofluorescence from small scale microscope-based studies to screening contexts. This could be useful for drug discovery, including studies of toxicology and efficacy, and for determining efficacy of particular therapeutic treatments,[31] e.g., for stratified medicine. It could also be applied to monitor stem cell differentiation.[13–17]

The instrument reported here could be further developed by combining the FLIM and phase contrast imaging with other imaging modalities. Indeed, spectrally resolved imaging of endogenous fluorescence from cell metabolites has previously been utilized for toxicology in an automated plate reader[42] and polarization resolved FLIM has been used to study the components of the complex NADH fluorescence signal in a laser scanning multiphoton microscope.[9] However, increasing the number of fluorescence parameters to be determined must also increase the required number of detected photons per pixel, which is challenging for live cell HCA, and we believe that FLIM combined with global fitting to a biexponential decay model is a good compromise between the

experimental limitations and the molecular information obtainable.

This instrument could also be improved by increasing the spatial resolution. Axial resolution could, in principle, be provided by implementing optical sectioning with wide-field time-gated FLIM using a Nipkow spinning disk, analogous to our previous work[3,19,41] but our current Nipkow spinning disk units are not designed for excitation wavelengths below 400 nm. Alternatively it may be possible to combine parallelized multiphoton excitation with wide-field FLIM[43,44] or TCSPC[45] to realize optical sectioning while avoiding the challenges associated with UV excitation, although our experience[44,45] suggests this would still result in longer image acquisition times. As discussed in Sec. 2.1, the lateral resolution of our instrument is currently limited by the resolution of the GOI in the current configuration. This could be improved using intensifiers that can resolve up to 30 lp/mm (resolution determined on precommercial prototype) or by changing the magnification, although this would decrease the field of view and therefore the numbers of cells to be imaged during HCA. With higher resolution, the mitochondria and cytoplasmic contributions could be separated using image segmentation and global fitting could be used to obtain lifetime components averaged over the same compartments across different cells. This would probably require the use of higher NA objectives with immersion fluid, which would add complexity to the instrument but has been realized in HCA plate readers.[46]

Acknowledgments

References

1. H. E. Grecco, P. Roda-Navarro, A. Girod, J. Hou, T. Frahm, D. C. Truxius, R. Pepperkok, A. Squire, P. I. H. Bastiaens, "*In situ* analysis of tyrosine phosphorylation networks by FLIM on cell arrays," *Nat. Methods* **7**, 467–472 (2010).

2. D. R. Matthews, G. O. Fruhwirth, G. Weitsman, L. M. Carlin, E. Ofo, M. Keppler, P. R. Barber, I. D. C. Tullis, B. Vojnovic, T. Ng, S. M. Ameer-Beg, "A multi-functional imaging approach to high-content protein interaction screening," *PLoS One* **7**, e33231 (2012).

3. D. Alibhai, D. J. Kelly, S. Warren, S. Kumar, A. Margineau, R. A. Serwa, E. Thinon, Y. Alexandrov, E. J. Murray, F. Stuhmeier, E. W. Tate, M. A. A. Neil, C. Dunsby, P. M. W. French, "Automated fluorescence lifetime imaging plate reader and its application to Förster resonant energy transfer readout of Gag protein aggregation," *J. Biophotonics* **6**, 398–408 (2013).

4. B. Chance, P. Cohen, F. Jobsis, B. Schoener, "Intracellular oxidation-reduction states *in vivo*," *Science* **137**, 499–508 (1962).

5. J. D. Shore, S. A. Evans, J. J. Holbrook, D. M. Parker, "NADH binding to porcine mitochondrial malate dehydrogenase," *J. Biol. Chem.* **254**, 9059–9062 (1979).

6. J. R. Lakowicz, "Principles of Fluorescence Spectroscopy," Springer, New York, (2006).

7. J. R. Lakowicz, H. Szmacinski, K. Nowaczyk, M. L. Johnson, "Fluorescence lifetime imaging of free and protein-bound NADH," *Proc. Natl. Acad. Sci. USA* **89**, 1271–1275 (1992).

8. N. D. Evans, L. Gnudi, O. J. Rolinski, D. J. S. Birch, J. C. Pickup, "Glucose-dependent changes in NAD (P)H-related fluorescence lifetime of adipocytes and fibroblasts *in vitro*: Potential for non-invasive glucose sensing in diabetes mellitus," *J. Photochem. Photobiol. B* **80**, 122–129 (2005).

9. H. D. Vishwasrao, A. A. Heikal, K. A. Kasischke, W. W. Webb, "Conformational dependence of intracellular NADH on metabolic state revealed by associated fluorescence anisotropy," *J. Biol. Chem.* **280**, 25119–25126 (2005).

10. A. Chorvatova, "Effect of ouabain on metabolic oxidative state in living cardiomyocytes evaluated by time-resolved spectroscopy of endogenous NAD (P)H fluorescence," *J. Biomed. Opt.* **17**, 101505 (2012).

11. N. Mazumder, R. K. Lyn, R. Singaravelu, A. Ridsdale, D. J. Moffatt, C.-W. Hu, H.-R. Tsai, J. McLauchlan, A. Stolow, F.-J. Kao, J. P. Pezacki, "Fluorescence lifetime imaging of alterations to cellular metabolism by domain 2 of the hepatitis C virus core protein," *PLoS One* **8**, e66738 (2013).

12. M. C. Skala, K. M. Riching, A. Gendron-Fitzpatrick, J. Eickhoff, K. W. Eliceiri, J. G. White, N. Ramanujam, "*In vivo* multiphoton microscopy of NADH and FAD redox states, fluorescence lifetimes, and cellular morphology in precancerous epithelia," *Proc. Natl. Acad. Sci. USA* **104**, 19494–19499 (2007).

13. S. Sikder, J. M. G. Reyes, C. S. Moon, O. Suwan-Apichon, J. H. Elisseeff, R. S. Chuck, "Noninvasive mitochondrial imaging in live cell culture," *Photochem. Photobiol.* **81**, 1569–1571 (2005).

14. K. König, A. Uchugonova, E. Gorjup, "Multiphoton fluorescence lifetime imaging of 3D-stem cell spheroids during differentiation," *Microsc. Res. Tech.* **74**, 9–17 (2011).

15. H.-W. Guo, C.-T. Chen, Y.-H. Wei, O. K. Lee, V. Gukassyan, F.-J. Kao, H.-W. Wang, "Reduced nicotinamide adenine dinucleotide fluorescence lifetime separates human mesenchymal stem cells from differentiated progenies," *J. Biomed. Opt.* **13**, 050505 (2011).

16. J. M. Squirrell, J. J. Fong, C. A. Ariza, A. Mael, K. Meyer, N. K. Shevde, A. Roopra, G. E. Lyons, T. J. Kamp, K. W. Eliceiri, B. M. Ogle, "Endogenous fluorescence signatures in living pluripotent stem cells change with loss of potency," *PLoS One* **7**, e43708 (2012).

17. B. K. Wright, L. M. Andrews, J. Markham, M. R. Jones, C. Stringari, M. A. Digman, E. Gratton, "NADH distribution in live progenitor stem cells by phasor-fluorescence lifetime image microscopy," *Biophys. J.* **103**, L7–L9 (2012).

18. A. Esposito, C. P. Dohm, M. Ba, F. S. Wouters, "Unsupervised fluorescence lifetime imaging microscopy for high content and high throughput screening," *Mol. Cell. Proteomics* **6**, 1446–1454 (2007).

19. C. B. Talbot, J. McGinty, D. M. Grant, E. J. McGhee, D. M. Owen, W. Zhang, T. D. Bunney, I. Munro, B. Isherwood, R. Eagle, A. Hargreaves, M. Katan, C. Dunsby, M. A. A. Neil, P. M. W. French, "High speed unsupervised fluorescence lifetime imaging confocal multiwell plate reader for high content analysis," *J. Biophotonics* **1**, 514–521 (2008).

20. C. Allan, J.-M. Burel, J. Moore, C. Blackburn, M. Linkert, S. Loynton, D. Macdonald, W. J. Moore, C. Neves, A. Patterson, M. Porter, A. Tarkowska, B. Loranger, J. Avondo, I. Lagerstedt, L. Lianas, S. Leo *et al.*, "OMERO: Flexible, model-driven data management for experimental biology," *Nat. Methods* **9**, 245–253 (2012).

21. F. Ambriz-Colin, M. Torres-Cisneros, J. G. Avina-Cervantes, J. E. Saavedra-Martinez, O. Debeir, J. J. Sanchez-Mondragon, "Detection of biological cells in phase-contrast video microscopy," *2006 Multi-conference Electron. Photonics*, pp. 239–243, IEEE (2006), doi: 10.1109/MEP.2006.335672.

22. A. E. Carpenter, T. R. Jones, M. R. Lamprecht, C. Clarke, I. H. Kang, O. Friman, D. A. Guertin, J. H. Chang, R. A. Lindquist, J. Moffat, P. Golland, D. M. Sabatini, "CellProfiler: Image analysis software for identifying and quantifying cell phenotypes," *Genome Biol.* **7**, R100 (2006).

23. A. W. Krause, W. W. Carley, W. W. Webb, "Fluorescent erythrosine B is preferable to trypan blue as a vital exclusion dye for mammalian cells in monolayer culture," *J. Histochem. Cytochem.* **32**, 1084–1090 (1984).

24. S. C. Warren, A. Margineanu, D. Alibhai, D. J. Kelly, C. Talbot, Y. Alexandrov, I. Munro, M. Katan, C. Dunsby, P. M. W. French, "Rapid global fitting of large fluorescence lifetime imaging microscopy datasets," *PLoS One* **8**, e70687 (2013).

25. M. Zuker, A. G. Szabo, L. Bramall, D. T. Krajcarski, B. Selinger, "Delta function convolution method (DFCM) for fluorescence decay experiments," *Rev. Sci. Instrum.* **56**, 14 (1985).

26. N. Pokala, "dunnett.m" *MATLAB Cent. File Exch.* (2012), Available at <http://www.mathworks.co.uk/matlabcentral/fileexchange/38157-dunnett-m>.

27. T. G. Scott, R. D. Spencer, N. J. Leonard, G. Weber, "Synthetic spectroscopic models related to coenzymes and base pairs. V. Emission properties of NADH. Studies of fluorescence lifetimes and quantum efficiencies of NADH, AcPyADH, [reduced acetylpyridineadenine dinucleotide] and simplified synthetic models," *J. Am. Chem. Soc.* **92**, 687–695 (1970).

28. T. P. Gonnella, J. M. Keating, J. A. Kjemhus, M. J. Picklo, J. P. Biggane, "Fluorescence lifetime analysis and effect of magnesium ions on binding of NADH to human aldehyde dehydrogenase 1," *Chem. Biol. Interact.* **202**, 85–90 (2013).

29. I. Georgakoudi, K. P. Quinn, "Optical imaging using endogenous contrast to assess metabolic state," *Annu. Rev. Biomed. Eng.* **14**, 351–367 (2012).

30. H.-W. Wang, V. Gukassyan, C.-T. Chen, Y.-H. Wei, H.-W. Guo, J.-S. Yu, F.-J. Kao, "Differentiation of apoptosis from necrosis by dynamic changes of reduced nicotinamide adenine dinucleotide fluorescence lifetime in live cells," *J. Biomed. Opt.* **13**, 054011 (2008).

31. A. J. Walsh, R. S. Cook, H. C. Manning, D. J. Hicks, A. Lafontant, C. L. Arteaga, M. C. Skala, "Optical metabolic imaging identifies glycolytic levels, sub-types

and early treatment response in breast cancer," *Cancer Res.* **73**, 6164–6174 (2013).

32. M. A. Digman, V. R. Caiolfa, M. Zamai, E. Gratton, "The Phasor approach to fluorescence lifetime imaging analysis," *Biophys. J.* **94**, 14–16 (2008).

33. Q. Yu, A. A. Heikal, "Two-photon autofluorescence dynamics imaging reveals sensitivity of intracellular NADH concentration and conformation to cell physiology at the single-cell level," *J. Photochem. Photobiol. B* **95**, 46–57 (2009).

34. W. Zheng, D. Li, J. Y. Qu, "Monitoring changes of cellular metabolism and microviscosity *in vitro* based on time-resolved endogenous fluorescence and its anisotropy decay dynamics," *J. Biomed. Opt.* **15**, 037013 (2010).

35. Z. H. Siddik, "Cisplatin: Mode of cytotoxic action and molecular basis of resistance," *Oncogene* **22**, 7265–7279 (2003).

36. W. M. Bonner, C. E. Redon, J. S. Dickey, A. J. Nakamura, O. A. Sedelnikova, S. Solier, Y. Pommier, "γ H2AX and cancer," **8**, 957–967 (2008).

37. E. M. Saleh, R. A. El-Awady, N. Anis, N. El-Sharkawy, "Induction and repair of DNA double-strand breaks using constant-field gel electrophoresis and apoptosis as predictive markers for sensitivity of cancer cells to cisplatin," *Biomed. Pharmacother.* **66**, 554–562 (2012).

38. H. Alborzinia, S. Can, P. Holenya, C. Scholl, E. Lederer, I. Kitanovic, S. Wölfl, "Real-time monitoring of cisplatin-induced cell death," *PLoS One* **6**, e19714 (2011).

39. M. C. Skala, K. M. Riching, D. K. Bird, A. Gendron-Fitzpatrick, J. Eickhoff, K. W. Eliceiri, P. J. Keely, N. Ramanujam, "*In vivo* multiphoton fluorescence lifetime imaging of protein-bound and free nicotinamide adenine dinucleotide in normal and precancerous epithelia," *J. Biomed. Opt.* **12**, 024014 (2007).

40. J.-S. Yu, H.-W. Guo, C.-H. Wang, Y.-H. Wei, H.-W. Wang, "Increase of reduced nicotinamide adenine dinucleotide fluorescence lifetime precedes mitochondrial dysfunction in staurosporine-induced apoptosis of HeLa cells," *J. Biomed. Opt.* **16**, 036008 (2011).

41. S. Kumar, D. Alibhai, A. Margineanu, R. Laine, G. Kennedy, J. McGinty, S. Warren, D. Kelly, Y. Alexandrov, I. Munro, C. Talbot, D. W. Stuckey, C. Kimberly, B. Viellerobe, F. Lacombe, E. W.-F. Lam, H. Taylor *et al.*, "FLIM FRET technology for drug discovery: Automated multiwell-plate high-content analysis, multiplexed readouts and application *in situ*," *Chemphyschem* **12**, 609–626 (2011).

42. A. Bednarkiewicz, R. M. Rodrigues, M. P. Whelan, "Non-invasive monitoring of cytotoxicity based on

kinetic changes of cellular autofluorescence," *Toxicol. In Vitro* **25**, 2088–2094 (2011).

43. S. Lévêque-Fort, M. P. Fontaine-Aupart, G. Roger, P. Georges, "Fluorescence-lifetime imaging with a multifocal two-photon microscope," *Opt. Lett.* **29**, 2884–2886 (2004).

44. R. Benninger, O. Hofmann, J. McGinty, J. Requejo-Isidro, I. Munro, M. Neil, A. Demello, P. French, "Time-resolved fluorescence imaging of solvent interactions in microfluidic devices," *Opt. Express* **13**, 6275–6285 (2005).

45. S. Kumar, C. Dunsby, P. A. A. De Beule, D. M. Owen, U. Anand, P. M. P. Lanigan, R. K. P. Benninger, D. M. Davis, M. A. A. Neil, P. Anand, C. Benham, A. Naylor, P. M. W. French, "Multifocal multiphoton excitation and time correlated single photon counting detection for 3-D fluorescence lifetime imaging," *Opt. Express* **15**, 12548–12561 (2007).

46. U. Liebel, S. Winkler, F. Sieckmann, "Immersion objective, apparatus for forming an immersion film and method," (2012).